

# *Beyond rattling: tetrahedrites as incipient ionic conductors*

Article

Published Version

Creative Commons: Attribution 4.0 (CC-BY)

Open Access

Mukherjee, Shriparna, Voneshen, David J., Duff, Andrew, Goodard, Pooja, Powell, Anthony V. and Vaqueiro, Paz ORCID logo ORCID: <https://orcid.org/0000-0001-7545-6262> (2023) Beyond rattling: tetrahedrites as incipient ionic conductors. *Advanced Materials*, 35 (44). 2306088. ISSN 1521-4095 doi: <https://doi.org/10.1002/adma.202306088> Available at <https://centaur.reading.ac.uk/112937/>

It is advisable to refer to the publisher's version if you intend to cite from the work. See [Guidance on citing](#).

To link to this article DOI: <http://dx.doi.org/10.1002/adma.202306088>

Publisher: Wiley

All outputs in CentAUR are protected by Intellectual Property Rights law, including copyright law. Copyright and IPR is retained by the creators or other copyright holders. Terms and conditions for use of this material are defined in the [End User Agreement](#).

[www.reading.ac.uk/centaur](http://www.reading.ac.uk/centaur)

**CentAUR**

Central Archive at the University of Reading

Reading's research outputs online

# Beyond Rattling: Tetrahedrites as Incipient Ionic Conductors

Shriparna Mukherjee, David J. Voneshen,\* Andrew Duff, Pooja Goddard, Anthony V. Powell, and Paz Vaquero\*

Materials with ultralow thermal conductivity are crucial to many technological applications, including thermoelectric energy harvesting, thermal barrier coatings, and optoelectronics. Liquid-like mobile ions are effective at disrupting phonon propagation, hence suppressing thermal conduction. However, high ionic mobility leads to the degradation of liquid-like thermoelectric materials under operating conditions due to ion migration and metal deposition at the cathode, hindering their practical application. Here, a new type of behavior, incipient ionic conduction, which leads to ultralow thermal conductivity, while overcoming the issues of degradation inherent in liquid-like materials, is identified. Using neutron spectroscopy and molecular dynamics (MD) simulations, it is demonstrated that in tetrahedrite, an established thermoelectric material with a remarkably low thermal conductivity, copper ions, although mobile above 200 K, are predominantly confined to cages within the crystal structure. Hence the undesirable migration of cations to the cathode can be avoided. These findings unveil a new approach for the design of materials with ultralow thermal conductivity, by exploring systems in which incipient ionic conduction may be present.

## 1. Introduction

Conversion of waste heat into electricity, which is facilitated by thermoelectric power generators, offers significant opportunities to reduce fossil fuel consumption and greenhouse gas emissions.<sup>[1]</sup> The efficiency of thermoelectric energy recovery depends on the figure of merit of the materials used in thermoelectric devices. Since the figure of merit ( $ZT = S^2\sigma T/\kappa$ ) is defined in terms of the Seebeck coefficient ( $S$ ), the electrical conductivity ( $\sigma$ ), and the total thermal conductivity ( $\kappa$ ), materials with low thermal conductivity are essential to maintain a temperature gradient. Both electrons and phonons contribute to thermal transport. The electronic contribution to the thermal conductivity ( $\kappa_e$ ) is directly related to the electrical conductivity by the Wiedemann–Franz law, hence reductions in  $\kappa_e$  necessarily involve an undesirable reduction in  $\sigma$ . Therefore, strategies to reduce thermal transport in thermoelectric materials

(and hence increase  $ZT$ ) focus primarily on the lattice component of the thermal conductivity ( $\kappa_l$ ), which is due to phonons.<sup>[2]</sup>

Among the approaches that have been explored to reduce  $\kappa_l$ ,<sup>[2]</sup> the phonon-liquid electron-crystal (PLEC) strategy,<sup>[3]</sup> which aims to lower  $\kappa_l$  below that of glass by exploiting the “liquid-like” behavior of superionic conductors, has been particularly successful.<sup>[4]</sup> PLEC (sometimes termed liquid-like) materials consist of a sub-lattice of immobile ions and a second liquid-like sub-lattice of mobile cations that disrupts phonon propagation. This class of material, exemplified by  $\text{Cu}_{2-x}\text{S}_{0.5}\text{Se}_{0.5}$  ( $ZT = 2.3$  at 1000 K for  $x = 0.06$ ),<sup>[5]</sup> exhibits outstanding thermoelectric performance, owing to an intrinsically ultralow  $\kappa_l$  ( $<0.5 \text{ W m}^{-1} \text{ K}^{-1}$ ). Unfortunately, the electric field created by the temperature gradient across a PLEC material during the operation of a thermoelectric device, results in ion migration, metal deposition, and ultimately material degradation, presenting a barrier to the practical application of these materials.<sup>[4,6]</sup> Here, we identify a new type of behavior which we term incipient ionic conduction, that leads to ultralow lattice thermal conductivities whilst obviating the degradation in thermoelectric performance that is an inevitable consequence of high cation mobility in liquid-like materials. We define incipient ionic conductors as materials on the verge of ionic conduction, containing ions with appreciable mobility, but in which long-range ionic diffusion is suppressed due to the trapping effect of the underlying crystal structure. We have exploited a combination of neutron spectroscopy and MD


S. Mukherjee, A. V. Powell, P. Vaquero  
Department of Chemistry, University of Reading  
Whiteknights  
Reading RG6 6DX, UK  
E-mail: p.vaquero@reading.ac.uk

D. J. Voneshen  
ISIS Pulsed Neutron and Muon Source  
Rutherford Appleton Laboratory  
Chilton, Didcot, Oxon OX11 0QX, UK  
E-mail: david.voneshen@stfc.ac.uk

D. J. Voneshen  
Department of Physics  
Royal Holloway University of London  
Egham TW20 0EX, UK

A. Duff  
Scientific Computing Department  
STFC Daresbury Laboratory  
Warrington WA4 4AD, UK

P. Goddard  
Department of Chemistry  
Loughborough University  
Loughborough LE11 3TU, UK

 The ORCID identification number(s) for the author(s) of this article can be found under <https://doi.org/10.1002/adma.202306088>

© 2023 The Authors. Advanced Materials published by Wiley-VCH GmbH. This is an open access article under the terms of the Creative Commons Attribution License, which permits use, distribution and reproduction in any medium, provided the original work is properly cited.

DOI: 10.1002/adma.202306088

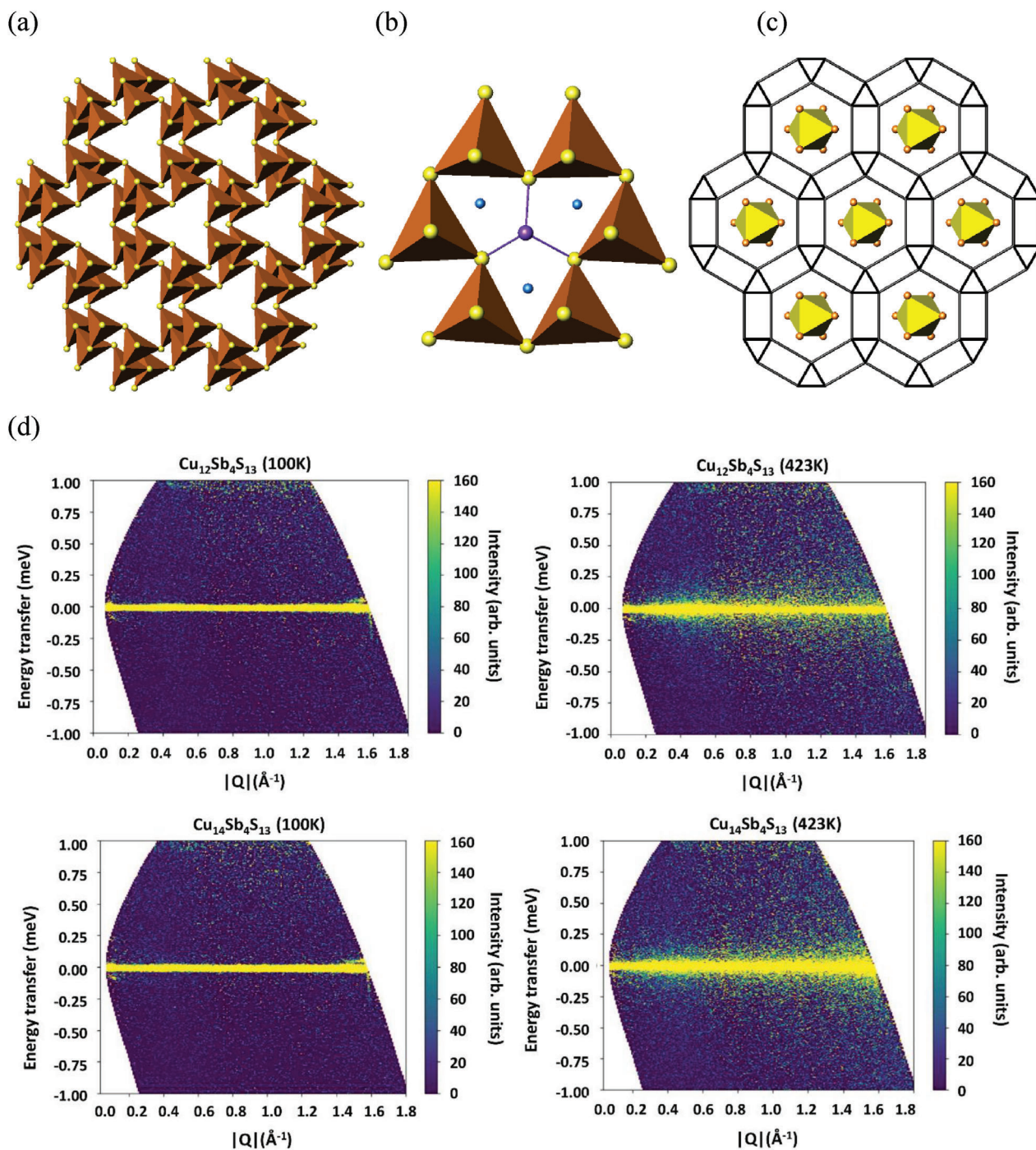


**Figure 1.** a) The collapsed sodalite framework, formed by Cu(1)S<sub>4</sub> tetrahedra (orange), found in the crystal structure of tetrahedrite. View along [111]. b) A window of a sodalite cage, showing the location of the SbS<sub>3</sub> trigonal pyramids and the interstitial Cu(3) site. c) Schematic representation of the sodalite framework, showing the SCu(2)<sub>6</sub> octahedra (yellow) located inside the sodalite cages. Each node in the sodalite framework represents a Cu(1)S<sub>4</sub> tetrahedron. View along [111]. Key: S, yellow spheres; Cu(2), orange spheres; Cu(3) blue spheres; Sb, purple spheres. d) QENS intensity color map for E<sub>i</sub> = 1.45 meV (instrumental resolution is 0.022 meV) of Cu<sub>12</sub>Sb<sub>4</sub>S<sub>13</sub> and Cu<sub>14</sub>Sb<sub>4</sub>S<sub>13</sub> at 100 and 423 K.

simulations to reveal that tetrahedrite, previously reported as a promising *p*-type thermoelectric material with intrinsically low thermal conductivity,<sup>[7,8]</sup> is an example of an incipient ionic conductor.

Tetrahedrite, Cu<sub>12</sub>Sb<sub>4</sub>S<sub>13</sub>, crystallizes in a collapsed sodalite structure,<sup>[9]</sup> in which corner-sharing Cu(1)S<sub>4</sub> tetrahedra form cages (Figure 1a), with SbS<sub>3</sub> trigonal pyramids located at the windows of each cage (Figure 1b). Inside each sodalite-type cage,

there is a  $\text{SCu}(2)_6$  unit in which a sulfur anion is octahedrally coordinated to six trigonal-planar copper cations (Figure 1c). Stoichiometric tetrahedrites can be formulated as  $\text{A}_6(\text{A},\text{B})_6\text{C}_4\text{Q}_{13}$  (where A is a monovalent transition metal, B a divalent transition metal, C a pnictogen, and Q a chalcogen),<sup>[10]</sup> but the crystal structure of tetrahedrite can accommodate two additional copper cations per formula unit at interstitial sites (Figure 1b); this expands the unit cell volume by  $\approx 3.5\%$ .<sup>[11]</sup> The incorporation of additional copper in copper-rich tetrahedrites,  $\text{Cu}_{12+x}\text{Sb}_4\text{S}_{13}$  ( $0 < x \leq 2.0$ ), leads to copper ionic mobility, the onset of which occurs at 393 K.<sup>[11]</sup> A variable-temperature neutron diffraction study demonstrates that at this temperature partial melting of the copper sublattice occurs. At 393 K, there is an anomaly in the lattice parameters, accompanied by marked changes in the temperature dependence of the electrical and thermal conductivities of the copper-rich phases.<sup>[11]</sup> While copper-rich tetrahedrites are ionic conductors,<sup>[12]</sup> studies on tetrahedrites of the type  $\text{Cu}_{12-x}\text{B}_x\text{Sb}_4\text{S}_{13}$  have concluded that copper ionic conductivity is restricted to the copper-rich phases.<sup>[13,14]</sup> Following the report by Suekuni and co-workers of the glass-like thermal conductivity of tetrahedrites,<sup>[15,16]</sup> it is now well established that these materials exhibit intrinsically low lattice thermal conductivities ( $\kappa_l < 1 \text{ W m}^{-1} \text{ K}^{-1}$  at room temperature), which approach the calculated minimum value.<sup>[8]</sup> In the case of copper-rich tetrahedrites,  $\text{Cu}_{12+x}\text{Sb}_4\text{S}_{13}$  ( $0 < x \leq 2.0$ ), it has been shown that the total thermal conductivity decreases with increasing copper content, reaching a value of  $\approx 0.4 \text{ W m}^{-1} \text{ K}^{-1}$  at room temperature for  $\text{Cu}_{14}\text{Sb}_4\text{S}_{13}$ .<sup>[11]</sup>

To date, the intrinsically low thermal conductivity of stoichiometric  $\text{Cu}_{12}\text{Sb}_4\text{S}_{13}$  has been attributed to rattling vibrations of the trigonal-planar copper cations, which are suppressed at low temperatures by a Jahn–Teller distortion.<sup>[17]</sup> It has been suggested that weak bonding interactions of  $\text{Cu}(2)$  with the lone pairs of two neighboring antimony cations drive rattling,<sup>[18]</sup> and that chemical pressure squeezes the  $\text{Cu}(2)$  cation out of planar coordination.<sup>[19]</sup>

Here, we sought to compare the behavior of a copper-rich tetrahedrite,  $\text{Cu}_{14}\text{Sb}_4\text{S}_{13}$ , a known ionic conductor,<sup>[12]</sup> with  $\text{Cu}_{12}\text{Sb}_4\text{S}_{13}$ , where low  $\kappa_l$  has been attributed to localized copper vibrations. Neutron spectroscopy measurements, using the LET spectrometer at the ISIS Facility,<sup>[20]</sup> were exploited to probe simultaneously copper diffusion through quasielastic neutron scattering (QENS) and the lattice dynamics through inelastic neutron scattering (INS). Analysis of these data provides unequivocal evidence of copper ion diffusion in both materials, with the motion predominantly confined to the sodalite cages.

## 2. Results and Discussion

A comparison of the QENS for both materials (Figure 1d) reveals marked changes with increasing temperature. While at 100 K data are resolution limited at the elastic scattering line ( $\Delta E = 0 \text{ meV}$ ), at 423 K the QENS signal increases considerably in both cases. As the onset of ionic mobility for  $\text{Cu}_{14}\text{Sb}_4\text{S}_{13}$  has been determined to be 393 K,<sup>[11]</sup> an increase in QENS intensity is expected, but the variation in QENS for  $\text{Cu}_{12}\text{Sb}_4\text{S}_{13}$  was unforeseen. Examination of the scans of energy transfer (Figure 2a) indicates that the QENS signal changes with temperature for both

materials. Up to 200 K, no broadening around  $\Delta E \approx 0 \text{ meV}$  is observed; the width of the elastic line is limited to the instrumental resolution of the LET spectrometer. By contrast, at temperatures of 200 K or above there is strong QENS broadening around the elastic peak. As copper has a significantly larger incoherent neutron cross-section than sulfur and antimony, and since at low energy transfer ( $< \pm 2 \text{ meV}$ ), QENS dominates the scattering, these data provide information on the copper motion. It should be noted that 200 K is below the known onset of copper ion mobility in copper-rich tetrahedrite but corresponds to the temperature at which an anomaly, of previously unknown origin, is observed in the electronic and lattice components of the thermal conductivity<sup>[15]</sup> as well as in the electrical resistivity measurements (Figure 2b).

For long-range (translational) diffusion, the full width at half maximum (FWHM) of the quasielastic Lorentzian component should follow a  $Q^2$ -law at small  $Q$  values and approach zero with decreasing  $Q$ .<sup>[21]</sup> For  $\text{Cu}_{12}\text{Sb}_4\text{S}_{13}$  and  $\text{Cu}_{14}\text{Sb}_4\text{S}_{13}$ , examination of the  $Q$ -dependence of the quasielastic broadening (Figure S1, Supporting Information) reveals that, at low  $Q$  values, the broadening of the QENS signal does not follow a  $Q^2$ -law and shows little  $Q$ -dependence; this is indicative of localized motion. To understand the origin of the QENS signal, atomistic simulations were performed between 100 and 700 K (in 100 K intervals). Long timescales ( $\approx \text{ns}$ ) are necessary to ensure that diffusion mechanisms that may operate over longer timescales are properly sampled. To achieve this, we performed classical MD simulations using interatomic potentials which were developed by fitting to density functional theory (DFT) data. The computed coefficient of thermal expansion between 400 and 600 K, is  $2.18 \times 10^{-5} \text{ K}^{-1}$ , close to the experimental value  $1.99 \times 10^{-5} \text{ K}^{-1}$  for copper-rich tetrahedrite,<sup>[11]</sup> confirming the validity of the potential used. The calculated QENS signal for the copper ions at temperatures comparable to those of the experimental data (Figure 2c), based on the MD simulations, is in excellent agreement with the experimental observations.

The simulations reveal a strongly correlated copper diffusion mechanism. In copper-rich tetrahedrite, copper ions that begin at interstitial  $\text{Cu}(3)$  sites vibrate, and after a time displace copper ions on neighboring crystallographic sites. The latter then become interstitial ions, while the former adopt the vacated crystallographic sites. This behavior is repeated, with each new  $\text{Cu}(3)$  interstitial ion vibrating, before displacing and taking the place of another copper ion. At 100 K, diffusion is negligible, in agreement with the QENS data. At 200 K the copper ions start moving between the corners of a  $\text{SCu}(2)_6$  octahedron (Figure 3a) in localized diffusional jumps in a confined octahedral environment, which do not result in long-range diffusion. The copper ions move between corners by passing above the center of the face of the octahedron, rather than moving along the edge. This behavior is illustrated in Figure 3b, which shows the displacement of a copper ion as a function of time. While at 100 K (black line), diffusion is negligible, at higher temperatures (red, blue, and purple lines), copper ions move only between the corners of a given  $\text{SCu}(2)_6$  octahedron ( $\approx 3.2 \text{ \AA}$  for adjacent corners and  $\approx 6 \text{ \AA}$  for opposite corners). Over much longer timescales, of the order of ns, the simulations for copper-rich tetrahedrite show long-range diffusion, consistent with the known ionic conductivity of this material.<sup>[12]</sup> This long-range diffusion involves the migration



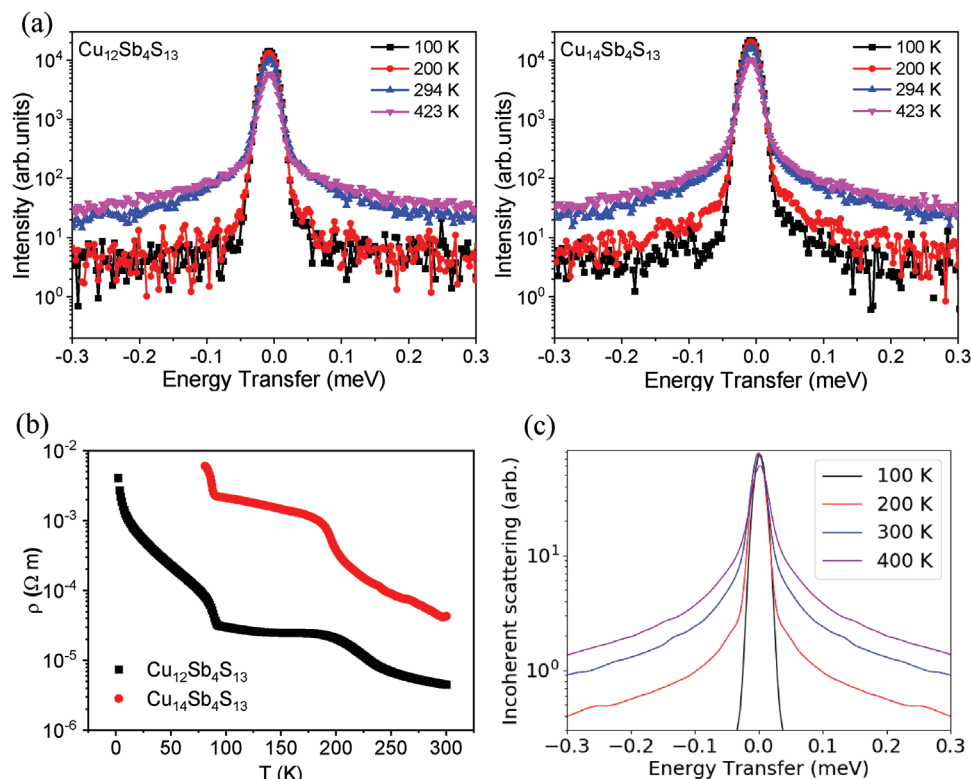


**Figure 2.** a) Scans of energy transfer for  $\text{Cu}_{12}\text{Sb}_4\text{S}_{13}$  and  $\text{Cu}_{14}\text{Sb}_4\text{S}_{13}$  at different temperatures. b) Electrical resistivity as a function of temperature. The anomaly at  $\approx 90$  K is related to a cubic-to-tetragonal phase transition.<sup>[17]</sup> c) Calculated scan of energy transfer for the copper ions in  $\text{Cu}_{14}\text{Sb}_4\text{S}_{13}$  as a function of temperature, based on the MD simulations.

of a copper ion from a given  $\text{SCu}(2)_6$  octahedron to a neighboring octahedron, with net diffusion governed by the timescale of migration between cages rather than the localized diffusional jumps within the cages. This suggests that the activation barrier to pass through the structural “bottleneck” that connects neighboring cages is significantly higher than the activation barrier for jumps within a given cage. As the long-range diffusion motion involving migration between cages is too slow for the time window of the LET spectrometer, the QENS data presented here only provide information on the localized diffusional jumps within the cages. A detailed study of the long-range copper diffusion in copper-rich tetrahedrite is ongoing and will be published in due course.

For  $\text{Cu}_{14}\text{Sb}_4\text{S}_{13}$  and  $\text{Cu}_{12}\text{Sb}_4\text{S}_{13}$ , the Q-dependence of the elastic incoherent structure factor (EISF), which represents the ratio of the elastic contribution to the total neutron scattering, is reasonably consistent with a diffusion model (see Supporting Information) in which the copper ions diffuse around the surface of an octahedron<sup>[22]</sup> (Figure 3c). This is the dominant mechanism for the temperatures and timescales investigated by the QENS measurements presented here. Using this octahedral model, the analysis of the QENS data suggests a residence time  $\tau = 17.6 \pm 0.6$  ps, which is reasonably close to that computed here from MD simulations,  $\tau = 31 \pm 4$  ps (for copper-rich tetrahedrite at 400 K). This level of agreement between experimental and calculated residence times is comparable to those reported in other studies of diffusion in ionic conductors.<sup>[23,24]</sup>

In  $\text{Cu}_{12}\text{Sb}_4\text{S}_{13}$ , this diffusive mode in which the copper ions diffuse around the surface of an octahedron, and which does not lead to net diffusion, accounts for the QENS signal. This is consistent with the prevalent view that there is no long-range diffusion in tetrahedrites with a 12:4 transition-metal: antimony ratio,  $\text{Cu}_{12-x}\text{B}_x\text{Sb}_4\text{S}_{13}$ . The stability and the effect of aging on the thermoelectric properties of  $\text{Cu}_{12-x}\text{B}_x\text{Sb}_4\text{S}_{13}$  phases have been previously discussed.<sup>[14,25]</sup> The absence of long-range diffusion in  $\text{Cu}_{12}\text{Sb}_4\text{S}_{13}$  is likely to be related to its smaller unit cell volume when compared to  $\text{Cu}_{14}\text{Sb}_4\text{S}_{13}$  ( $1100 \text{ \AA}^3$  for  $\text{Cu}_{12}\text{Sb}_4\text{S}_{13}$  and  $1140 \text{ \AA}^3$  for  $\text{Cu}_{14}\text{Sb}_4\text{S}_{13}$ , See Table S1, Supporting Information). In the latter, the unit cell volume expands to accommodate the two additional copper ions,<sup>[11]</sup> opening a diffusion pathway for inter-octahedra jumps of copper ions. Moreover, in tetrahedrites of the type  $\text{Cu}_{12-x}\text{B}_x\text{Sb}_4\text{S}_{13}$ , doping entails the substitution of the Cu(1) ions present in the framework with divalent transition ions,<sup>[8]</sup> which are likely to hinder diffusion pathways between cages.

A vibrational mode is observed at 3–4 meV in the INS data (Figure 4); this mode is also present in the INS computed from the MD simulations (Figure S2, Supporting Information). Comparison with previously published calculated phonon density of states,<sup>[18,26]</sup> which are in good agreement with those presented here (Figure S2, Supporting Information), indicates that this peak can be identified as a quasi-localized optical mode, predominantly associated with the trigonal-planar Cu(2) atoms. While this mode has been assigned to the out-of-plane rattling of the

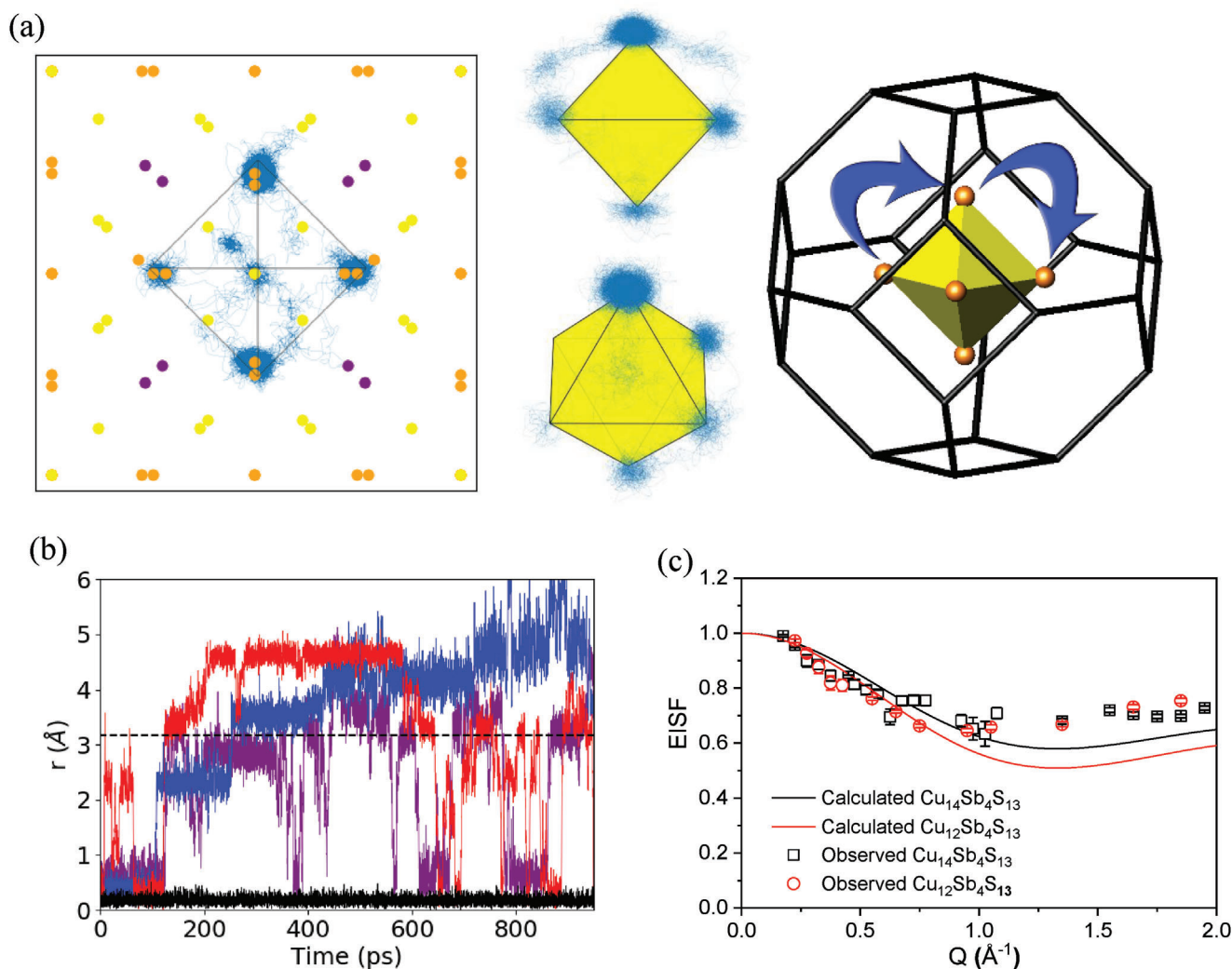


**Figure 3.** a) Left: 2D view of the MD simulation carried out at 400 K, illustrating the localized diffusion of copper ions, shown by the blue line, around a  $\text{SCu}(2)_6$  octahedron in copper-rich tetrahedrite. Middle: Two 3D views of the trajectory of a copper ion around a  $\text{SCu}(2)_6$  octahedron. Right: A  $\text{SCu}(2)_6$  octahedron inside a sodalite cage, with the jumps highlighted by blue arrows. Atom key as in Figure 1. b) Displacement of a selected copper ion in  $\text{Cu}_{14}\text{Sb}_4\text{S}_{13}$  as a function of time in the MD simulations. Black, red, blue, and purple lines correspond to simulations at 100, 200, 300, and 400 K respectively. The horizontal dashed line at 3.2 Å represents the distance between adjacent nearest-neighbor copper ions in a  $\text{SCu}(2)_6$  octahedron. c) Comparison of the experimentally-determined EISF for  $\text{Cu}_{14}\text{Sb}_4\text{S}_{13}$  (black squares) and  $\text{Cu}_{12}\text{Sb}_4\text{S}_{13}$  (red circles) at 423 K with the expected EISF (see SI) for localized diffusional jumps confined to an octahedron. The black and red lines show the expected EISF for  $\text{Cu}_{14}\text{Sb}_4\text{S}_{13}$  and  $\text{Cu}_{12}\text{Sb}_4\text{S}_{13}$ , respectively.

$\text{Cu}(2)$  atoms, the QENS and MD simulations results presented here indicate that at temperatures  $\geq 200$  K, instead of rattling, the  $\text{Cu}(2)$  atoms vibrate out of a corner of the  $\text{SCu}(2)_6$  octahedron to move to a neighboring corner. INS measurements on a single crystal have shown that there is a strong scattering process between the low-energy optical mode of the  $\text{Cu}(2)$  atoms and the transverse acoustic phonons.<sup>[27]</sup> This scattering process will disrupt the propagation of heat-carrying acoustic phonons. The higher energy of the low-energy optical mode for  $\text{Cu}_{14}\text{Sb}_4\text{S}_{13}$  when compared to  $\text{Cu}_{12}\text{Sb}_4\text{S}_{13}$  can be related to the area of the triangle formed by the three sulfur atoms coordinated to each  $\text{Cu}(2)$ . Reducing the area of this triangle increases the chemical pressure on  $\text{Cu}(2)$ , which in turn raises the amplitude of the vibration.<sup>[19]</sup> This mode shows significant softening on cooling (Figure 4c), revealing strong anharmonicity, and also broadens,

as the transition to the low-temperature tetragonal phase, which for  $\text{Cu}_{12}\text{Sb}_4\text{S}_{13}$  occurs at  $\approx 90$  K,<sup>[17]</sup> is approached. INS measurements below 90 K have shown that this low-energy mode disappears at the structural transition and then re-appears at a lower energy in the tetragonal phase.<sup>[28]</sup>

The exact mechanism by which the thermal conductivity of “liquid-like” superionic conductors is suppressed has been a matter of considerable debate. Initially, their ultralow thermal conductivity was attributed to the disappearance of the transverse acoustic phonon modes,<sup>[3]</sup> but it has been subsequently demonstrated that the hopping timescales of the mobile ions are significantly longer than the phonon relaxation times for the transverse phonon branches,<sup>[29]</sup> and that therefore the transverse phonon modes persist into the “liquid-like” state.<sup>[29–31]</sup> Instead, it appears that the remarkable thermal

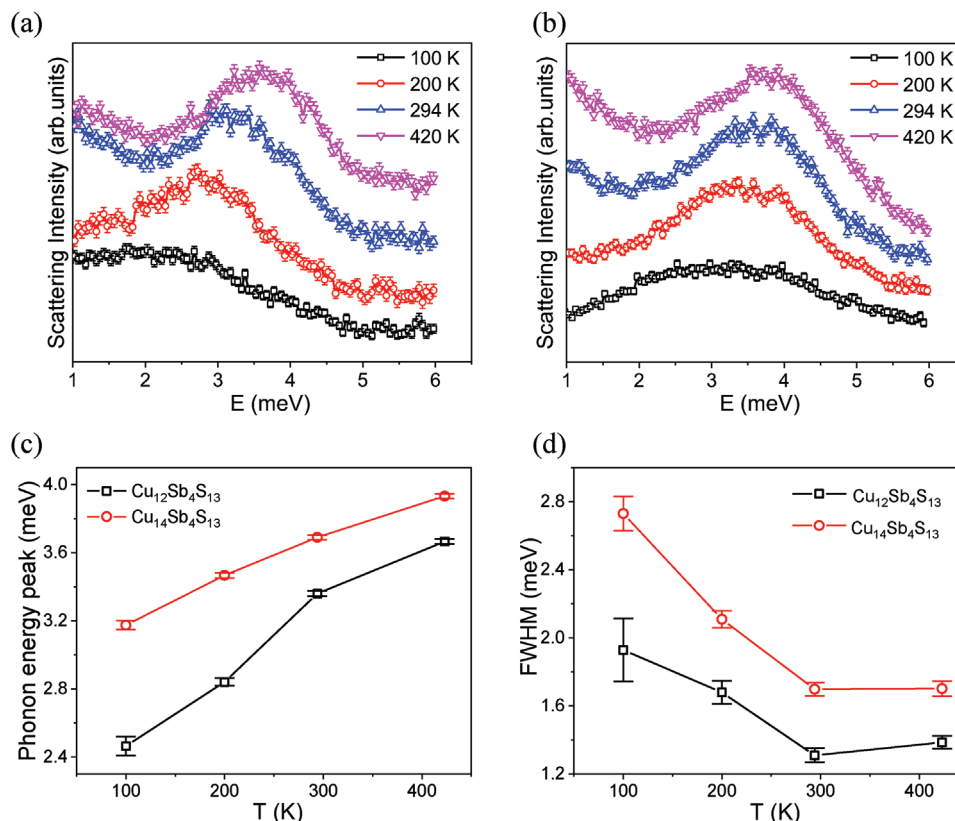


**Figure 4.** Low-energy phonon mode for a)  $\text{Cu}_{12}\text{Sb}_4\text{S}_{13}$  and b)  $\text{Cu}_{14}\text{Sb}_4\text{S}_{13}$ . Temperature dependence of c) the energy and d) the FWHM of the low-energy mode of the trigonal planar Cu(2) ions.

transport behavior of “liquid-like” superionic conductors is a consequence of strong anharmonicity.<sup>[29,30]</sup> Similarly to the findings on “liquid-like” superionic conductors, our INS measurements on tetrahedrite reveal strong anharmonicity in the low-energy optical mode of the Cu(2) ions. This anharmonicity is already present below 200 K, the temperature at which the localized diffusional jumps of the Cu(2) ions start. To achieve a deeper understanding of the interplay between the lattice dynamics and the localized diffusional jumps of the Cu(2) ions, single-crystal INS data as a function of temperature are required.

### 3. Conclusion

To conclude, these results demonstrate that in tetrahedrite, copper ions are mobile between 200 and 400 K but are largely confined to cages within the crystal structure. The analysis of the data presented here suggests that in  $\text{Cu}_{12-x}\text{B}_x\text{Sb}_4\text{S}_{13}$  the activation barrier to pass through the structural “bottleneck” that connects neighboring cages must be relatively high. For this reason, while the copper ions are mobile, they are largely trapped inside cages. The low-energy optical mode related to intra-cage copper diffusion is capable of strongly scattering the heat-carrying acoustic phonons and hence lowers the lattice thermal conductivity. This work reveals that tetrahedrite behaves as an incipient ionic conductor. We anticipate that the discovery of incipient ionic conduction reported here will open a new avenue for the search for

materials with ultralow thermal conductivity, without the degradation issues inherent to liquid-like materials. We envisage that data mining of crystallographic databases, which contain hundreds of thousands of experimentally-determined crystal structures, could be exploited to discover other materials with incipient ionic conductivity. For instance, low-cost computational approaches such as the bond–valence method could be used to identify materials containing cages in which the ion motion is confined to these cages.

### 4. Experimental Section

**Synthesis:** For  $\text{Cu}_{12}\text{Sb}_4\text{S}_{13}$ , a stoichiometric mixture of elemental Cu (Sigma Aldrich, –150 mesh, 99.5%), Sb (Alfa Aesar, –200 mesh, 99.5%), and sulfur flakes (Sigma Aldrich 99.99+%) was ground and the mixture sealed into an evacuated fused-silica tube. Using a heating rate of  $1 \text{ K min}^{-1}$ , the mixture was initially heated at 923 K for 5 h, followed by 48 h at 773 K. The furnace was then cooled to room temperature at  $0.5 \text{ K min}^{-1}$ . The ingot obtained was ground and cold-pressed into pellets. The cold-pressed pellets were sealed into an evacuated fused-silica tube and annealed at 773 K (heating rate  $1 \text{ K min}^{-1}$ ) for 2 days. The furnace was cooled to room temperature at a rate of  $0.5 \text{ K min}^{-1}$ . Following grinding, the powdered sample was again sealed into a fused-silica tube, heated at  $1 \text{ K min}^{-1}$  to 673 K, maintained at this temperature for 4 days, and subsequently slowly cooled to room temperature at  $0.2 \text{ K min}^{-1}$ .

For  $\text{Cu}_{14}\text{Sb}_4\text{S}_{13}$ , a stoichiometric mixture of the elements (total of 6 g), together with 40 stainless-steel balls with a diameter of 6 mm, were loaded



into a 25 ml stainless-steel jar. The mixture was ball milled at 500 rpm for 8 h using a Retsch PM100 ball mill. The black powder was sealed into an evacuated fused-silica tube and heated at a rate of 5 K min<sup>-1</sup> to 773 K; the sealed tube was held at this temperature for four days. This was followed by cooling to room temperature at 0.2 K min<sup>-1</sup>.

QENS data were collected on the as-prepared powders. For electrical resistivity measurements, the powders were consolidated into pellets by hot pressing at 723 K and 80 MPa for 30 min using a graphite mold of diameter 12.7 mm; pressure was released upon cooling. The procedure was carried out under a nitrogen flow to prevent oxidation.

**Characterization:** Powder X-ray diffraction data were collected on powder samples using a Bruker D8 Advance X-ray diffractometer, operating with Ge-monochromated Cu K $\alpha_1$  ( $\lambda = 1.54046 \text{ \AA}$ ) radiation (Figures S3 and S4, Supporting Information). Rietveld refinements to determine the lattice parameters were performed using GSAS (Table S1, Figures S5 and S6, Supporting Information). Analysis of the diffraction data indicated that the lattice parameters and the purity of the samples were in good agreement with those in previous reports.<sup>[11,14,15]</sup> For Cu<sub>14</sub>Sb<sub>4</sub>S<sub>13</sub>, the low-temperature electrical resistivity was measured on an ingot, cut from a hot-pressed pellet, with dimensions of 2 × 3 × 11 mm. Four probe connections were established using silver wires (50  $\mu\text{m}$  diameter) and colloidal silver paint. The four probes were connected to an HP34401A multimeter, and the sample was loaded into an Oxford Instruments CF1200 cryostat. The data were collected over the temperature range 80 ≤ T/K ≤ 300 in 1 K steps with temperature control effected with an ITC502 temperature controller. The low-temperature electrical resistivity for Cu<sub>12</sub>Sb<sub>4</sub>S<sub>13</sub> was measured in a PPMS system.<sup>[17]</sup>

**Neutron Spectroscopy:** Neutron scattering data were collected on the LET spectrometer (ISIS Neutron and Muon Source, UK).<sup>[32]</sup> The powder sample was loaded into an annular vanadium can. Data were collected at 100, 200, 294, and 423 K. LET was configured to incident energies of 1.45, 2.20, 3.70, 7.52, and 22.75 meV. Identical measurements were carried out for the empty aluminum can and the instrumental background was subtracted using the Mantid package.<sup>[33]</sup> The QENS data were analyzed using the Data Analysis and Visualization Environment (DAVE).<sup>[34]</sup> The QENS fitting curves obtained using DAVE are presented in the Supporting Information (Figure S7, Supporting Information). For each temperature, and at incident energies,  $E_i = 1.45, 2.20,$  and  $3.70 \text{ meV}$ , datasets ranging from  $0.2 \leq |Q|/\text{\AA}^{-1} \leq 2$  and  $-0.3 \leq \Delta E/\text{meV} \leq 0.3$  were extracted using Mantid (Mslice).<sup>[33]</sup> Each dataset was fitted using a delta function for the elastic line, which corresponded to the instrument resolution, together with a single Lorentzian to model the quasielastic energy broadening. The determination of the experimental and calculated EISF is described in the Supporting Information.

The INS data were integrated over the range 2 to 3  $\text{\AA}^{-1}$  in Q-space and in the neutron energy gain for the LET incident energy 7.52 meV. The normalized neutron-weighted phonon density of states was obtained using a custom Python script. Peaks were fitted using individual Gaussian functions in the DAVE package.

**Simulations:** The DFT training data were calculated using the VASP software package (version 5.4.4) and the projector augmented wave method<sup>[35–37]</sup> and consisted of energies, atomic forces, and stress tensors generated from ab initio MD simulations. A 58-atom cubic conventional Cu<sub>12</sub>Sb<sub>4</sub>S<sub>13</sub> cell was used, with two additional Cu atoms added to Cu(3) interstitial sites – corresponding to a Cu-rich tetrahedrite composition Cu<sub>14</sub>Sb<sub>4</sub>S<sub>13</sub>. Accordingly, quantitative predictions using this cell were directly relevant to experimentally-studied Cu<sub>14</sub>Sb<sub>4</sub>S<sub>13</sub>, since the reported crystal structure for this material contains Cu(3) interstitial sites.<sup>[11]</sup>

Ab initio MD simulations were performed across a range of temperatures, including 200, 500, 750, 1000, 2000, and 3000 K. Energies and forces allow the capture of lattice dynamics, while stress tensors allowed modeling of thermal expansion and captured the temperature-dependent elastic response. Temperatures higher than the window of interest ( $\geq 1000 \text{ K}$ ) were necessary to capture diffusion events, which were not observed at lower temperatures due to the limited length- and time-scales accessible to DFT ( $\approx \text{nm}$  and  $\approx \text{ps}$  respectively in the simulations for tetrahedrite). MD runs at each temperature were performed initially under constant pressure

for 1000 steps (with timestep 5 fs, total duration is 0.5 ps). Using the equilibrated lattice constants, a constant volume run was then performed for a further 1000 steps, providing the data to be used for training the potential. The PBE exchange-correlation functional (issued on September 6, 2000) was used throughout. For Cu, 3p, 4s, and 3d, for Sb, 5s and 5p, and for S, 3s and 3p electrons were included as valence states. A plane-wave cutoff of 500 eV and a grid of 2 × 2 × 2 Monkhorst–Pack k points was used, which provided an accuracy of 1 meV atom<sup>-1</sup>.

Potential optimization was performed using the MEAMfit code,<sup>[38]</sup> with the reference-free modified embedded atom method formalism employed to capture the strong directional bonding of tetrahedrite. For each temperature, every 15th atomic configuration of the constant pressure runs were used as training data. In total 400 configurations were used, with energies, force components, and stress tensor components totaling 72400 data-points. For uncertainty quantification, four potentials were optimized separately, using different numbers of terms in the pair-wise interactions (pair-potentials and densities considered separately) and/or different values of the maximum allowed value of the cut-off radius for these interactions. Representative values of the root mean squared errors of energies, forces, and stresses of the configurations used in the training database as calculated using one of these potentials with respect to DFT are: 8.07 meV atom<sup>-1</sup>; 0.178 eV  $\text{\AA}^{-1}$ ;  $1.636 \times 10^{-3} \text{ eV \AA}^{-1}$ . The development of the potentials, including setting up and analyzing the training set data, and setting up MEAMfit inputs, was handled by the automated potential development (APD) workflow.<sup>[39]</sup>

## Supporting Information

Supporting Information is available from the Wiley Online Library or from the author.

## Acknowledgements

The authors thank the Leverhulme Trust for Research Project Grant RPG-2019-288 for funding. The authors would also like to acknowledge the STFC ISIS Neutron and Muon Source for the provision of beam time on the LET beamline under proposal RB 1810207. The authors gratefully acknowledge funding from the Ada Lovelace Centre (ALC) at the Science and Technology Facilities Council (STFC) (proposals “APD digital asset for experimentalists and users of facilities” and “APD and deployment for ISIS users”). Through membership of the UK’s High-End Computing (HEC) Materials Chemistry Consortium, which was funded by EPSRC Grants No. EP/L000202 and No. EP/R029431, this work used the UK Materials and Molecular Modelling (MMM) Hub for computational resources, which was partially funded by EPSRC Grant No. EP/P020194. In addition, the authors are grateful for HPC support through the STFC Scientific Computing Department’s SCARF cluster.

## Conflict of Interest

The authors declare no conflict of interest.

## Data Availability Statement

The neutron scattering data that support the findings of this study are openly available in the ISIS Neutron and Muon Source Data Journal at <http://doi.org/10.5286/ISIS.E.90680555>.

## Keywords

ionic mobility, quasielastic neutron scattering, rattling, tetrahedrites, thermal conductivities, thermoelectric

Received: June 23, 2023  
Revised: August 4, 2023  
Published online: September 28, 2023

- [1] R. Freer, A. V. Powell, *J. Mater. Chem. C* **2020**, *8*, 441.
- [2] T. Ghosh, M. Dutta, D. Sarkar, K. Biswas, *J. Am. Chem. Soc.* **2022**, *144*, 10099.
- [3] H. Liu, X. Shi, F. Xu, L. Zhang, W. Zhang, L. Chen, Q. Li, C. Uher, T. Day, G. J. Snyder, *Nat. Mater.* **2012**, *11*, 422.
- [4] K. Zhao, P. Qiu, X. Shi, L. Chen, *Adv. Funct. Mater.* **2020**, *30*, 1903867.
- [5] K. Zhao, P. Qiu, Q. Song, A. B. Blichfeld, E. Eikeland, D. Ren, B. Ge, B. B. Iversen, X. Shi, L. Chen, *Mater. Today Phys.* **2017**, *1*, 14.
- [6] G. Dennler, R. Chmielowski, S. Jacob, F. Capet, P. Roussel, S. Zastrow, K. Nielsch, I. Opahle, G. K. H. Madsen, *Adv. Energy Mater.* **2014**, *4*, 1301581.
- [7] X. Lu, D. T. Morelli, Y. Xia, F. Zhou, V. Ozolins, H. Chi, X. Zhou, C. Uher, *Adv. Energy Mater.* **2013**, *3*, 342.
- [8] K. Suekuni, M. Ohta, T. Takabatake, E. Guilmeau, in *Thermoelectric Energy Conversion*, (Ed.: R. Funahashi), Woodhead Publishing, Cambridge **2021**, pp. 197.
- [9] N. E. Johnson, J. R. Craig, J. D. Rimstidt, *Am. Mineral.* **1988**, *73*, 389.
- [10] C. Biagioni, L. L. George, N. J. Cook, E. Makovicky, Y. Mořlo, M. Pasero, J. Sejkora, C. J. Stanley, M. D. Welch, F. Bosi, *Am. Mineral.* **2020**, *105*, 109.
- [11] P. Vaqueiro, G. Guřlou, A. Kaltzoglou, R. I. Smith, T. Barbier, E. Guilmeau, A. V. Powell, *Chem. Mater.* **2017**, *29*, 4080.
- [12] E. Makovicky, B. J. Skinner, *Can. Mineral.* **1979**, *17*, 619.
- [13] G. P. L. Guřlou, A. V. Powell, R. I. Smith, P. Vaqueiro, *J. Appl. Phys.* **2019**, *126*, 045107.
- [14] T. Barbier, P. Lemoine, S. Gascoin, O. I. Lebedev, A. Kaltzoglou, P. Vaqueiro, A. V. Powell, R. I. Smith, E. Guilmeau, *J. Alloys Compd.* **2015**, *634*, 253.
- [15] K. Suekuni, K. Tsuruta, T. Ariga, M. Koyano, *Appl. Phys. Express* **2012**, *5*, 051201.
- [16] K. Suekuni, H. I. Tanaka, F. S. Kim, K. Umeo, T. Takabatake, *J. Phys. Soc. Jpn.* **2015**, *84*, 103601.
- [17] S. O. Long, A. V. Powell, S. Hull, F. Orlandi, C. C. Tang, A. R. Supka, M. Fornari, P. Vaqueiro, *Adv. Funct. Mater.* **2020**, *30*, 1909409.
- [18] W. Lai, Y. Wang, D. T. Morelli, X. Lu, *Adv. Funct. Mater.* **2015**, *25*, 3648.
- [19] K. Suekuni, C. H. Lee, H. I. Tanaka, E. Nishibori, A. Nakamura, H. Kasai, H. Mori, H. Usui, M. Ochi, T. Hasegawa, M. Nakamura, S. Ohira-Kawamura, T. Kikuchi, K. Kaneko, H. Nishiate, K. Hashikuni, Y. Kosaka, K. Kuroki, T. Takabatake, *Adv. Mater.* **2018**, *30*, 1706230.
- [20] R. I. Bewley, J. W. Taylor, S. M. Bennington, *Nucl. Instrum. Methods Phys. Res. Sect. Accel. Spectrometers Detect. Assoc. Equip.* **2011**, *637*, 128.
- [21] J. P. Embs, F. Juranyi, R. Hempelmann, *Z. Für Phys. Chem.* **2010**, *224*, 5.
- [22] L. Cristofolini, P. Facci, M. P. Fontana, G. Cicognani, A. J. Dianoux, *Phys. Rev. B* **2000**, *61*, 3404.
- [23] M. K. Gupta, J. Ding, D. Bansal, D. L. Abernathy, G. Ehlers, N. C. Osti, W. G. Zeier, O. Delaire, *Adv. Energy Mater.* **2022**, *12*, 2200596.
- [24] M. J. Klenk, S. E. Boeberitz, J. Dai, N. H. Jalarvo, V. K. Peterson, W. Lai, *Solid State Ion* **2017**, *312*, 1.
- [25] R. Coelho, E. B. Lopes, A. P. Gonçalves, *J. Electron. Mater.* **2021**, *50*, 467.
- [26] J. Li, M. Zhu, D. L. Abernathy, X. Ke, D. T. Morelli, W. Lai, *APL Mater.* **2016**, *4*, 104811.
- [27] Y. Bouyrie, C. Candolfi, S. Pailhřs, M. M. Koza, B. Malaman, A. Dauscher, J. Tobola, O. Boiron, L. Saviot, B. Lenoir, *Phys. Chem. Chem. Phys.* **2015**, *17*, 19751.
- [28] A. F. May, O. Delaire, J. L. Niedziela, E. Lara-Curzio, M. A. Susner, D. L. Abernathy, M. Kirkham, M. A. McGuire, *Phys. Rev. B* **2016**, *93*, 064104.
- [29] D. J. Voneshen, H. C. Walker, K. Refson, J. P. Goff, *Phys. Rev. Lett.* **2017**, *118*, 145901.
- [30] J. L. Niedziela, D. Bansal, A. F. May, J. Ding, T. Lanigan-Atkins, G. Ehlers, D. L. Abernathy, A. Said, O. Delaire, *Nat. Phys.* **2019**, *15*, 73.
- [31] Q. Ren, M. K. Gupta, M. Jin, J. Ding, J. Wu, Z. Chen, S. Lin, O. Fabelo, J. A. Rodríguez-Velamazán, M. Kofu, K. Nakajima, M. Wolf, F. Zhu, J. Wang, Z. Cheng, G. Wang, X. Tong, Y. Pei, O. Delaire, J. Ma, *Nat. Mater.* **2023**, *22*, 999.
- [32] P. Vaqueiro, D. Voneshen, A. V. Powell, "Phonon-liquid electron-crystal behaviour in copper-rich tetrahedrites," can be found under <http://doi.org/10.5286/ISIS.E.90680555>.
- [33] O. Arnold, J. C. Bilheux, J. M. Borreguero, A. Buts, S. I. Campbell, L. Chapon, M. Doucet, N. Draper, R. Ferraz Leal, M. A. Gigg, V. E. Lynch, A. Markvardsen, D. J. Mikkelson, R. L. Mikkelson, R. Miller, K. Palmen, P. Parker, G. Passos, T. G. Perring, P. F. Peterson, S. Ren, M. A. Reuter, A. T. Savici, J. W. Taylor, R. J. Taylor, R. Tolchenov, W. Zhou, J. Zikovsky, *Nucl. Instrum. Methods Phys. Res. Sect. Accel. Spectrometers Detect. Assoc. Equip.* **2014**, *764*, 156.
- [34] R. T. Azuah, L. R. Kneller, Y. Qiu, P. L. W. Tregenna-Piggott, C. M. Brown, J. R. D. Copley, R. M. Dimeo, *J. Res. Natl. Inst. Stand. Technol.* **2009**, *114*, 341.
- [35] G. Kresse, J. Hafner, *Phys. Rev. B* **1993**, *47*, 558.
- [36] G. Kresse, J. Furthmüller, *Comput. Mater. Sci.* **1996**, *6*, 15.
- [37] G. Kresse, J. Furthmüller, *Phys. Rev. B* **1996**, *54*, 11169.
- [38] A. I. Duff, M. Finnis, P. Murgis, B. J. Thijsse, M. H. Sluiter, *Comput. Phys. Commun.* **2015**, *196*, 439.
- [39] A. I. Duff, R. Sakidja, H. Walker, R. Ewings, D. Voneshen, *Comput. Phys. Commun.* **2023**, *293*, 108896.